Evaluation of Automatically Quantified Foveal Avascular Zone Metrics for Diagnosis of Diabetic Retinopathy Using Optical Coherence Tomography Angiography

Yansha Lu,[1,2] Joseph M. Simonett,[1] Jie Wang,[1] Miao Zhang,[1,3] Thomas Hwang,[1] Ahmed M. Hagag,[1] David Huang,[1] Dengwang Li,[2] and Yali Jia[1]

[1]Casey Eye Institute, Oregon Health & Science University, Portland, Oregon, United States
[2]Shandong Province Key Laboratory of Medical Physics and Image Processing Technology, Institute of Biomedical Sciences, School of Physics and Electronics, Shandong Normal University, Jinan, China
[3]Optovue, Inc., Fremont, California, United States

Correspondence: Yali Jia, Casey Eye Institute, Oregon Health & Science University, Portland, OR 97239, USA; jiaya@ohsu.edu.
Dengwang Li, School of Physics and Electronics, Shandong Normal University, Jinan 250014, China; dengwang@sdnu.edu.cn.

YL and JMS contributed equally to the work presented here and should therefore be regarded as equivalent authors.

Submitted: November 30, 2017
Accepted: March 19, 2018

Citation: Lu Y, Simonett JM, Wang J, et al. Evaluation of automatically quantified foveal avascular zone metrics for diagnosis of diabetic retinopathy using optical coherence tomography angiography. *Invest Ophthalmol Vis Sci*. 2018;59:2212–2221. https://doi.org/10.1167/iovs.17-23498

Purpose. To describe an automated algorithm to quantify the foveal avascular zone (FAZ), using optical coherence tomography angiography (OCTA), and to compare its performance for diagnosis of diabetic retinopathy (DR) and association with best-corrected visual acuity (BCVA) to that of extrafoveal avascular area (EAA).

Methods. We obtained 3 × 3-mm macular OCTA scans in diabetic patients with various levels of DR and healthy controls. An algorithm based on a generalized gradient vector flow (GGVF) snake model detected the FAZ, and metrics assessing FAZ size and irregularity were calculated. We compared the automated FAZ segmentation to manual delineation and tested the within-visit repeatability of FAZ metrics. The correlations of two conventional FAZ metrics, two novel FAZ metrics, and EAA with DR severity and BCVA, as determined by Early Treatment Diabetic Retinopathy Study (ETDRS) charts, were assessed.

Results. Sixty-six eyes from 66 diabetic patients and 19 control eyes from 19 healthy participants were included. The agreement between manual and automated FAZ delineation had a Jaccard index > 0.82, and the repeatability of automated FAZ detection was excellent in eyes at all levels of DR severity. FAZ metrics that incorporated both FAZ size and shape irregularity had the strongest correlation with clinical DR grade and BCVA. Of all the tested OCTA metrics, EAA had the greatest sensitivity in differentiating diabetic eyes without clinical evidence of retinopathy, mild to moderate nonproliferative DR (NPDR), and severe NPDR to proliferative DR from healthy controls.

Conclusions. The GGVF snake algorithm tested in this study can accurately and reliably detect the FAZ, using OCTA data at all DR severity grades, and may be used to obtain clinically useful information from OCTA data regarding macular ischemia in patients with diabetes. While FAZ metrics can provide clinically useful information regarding macular ischemia, and possibly visual acuity potential, EAA measurements may be a better biomarker for DR.

Keywords: optical coherence tomography, diabetic retinopathy, microcirculation, OCT angiography

Diabetic macular ischemia (DMI) is a clinically important finding in diabetic retinopathy (DR) and correlates closely with vision loss.[1–3] Fluorescein angiography (FA) has long been the standard imaging modality for the qualitative evaluation of DMI, particularly the foveal avascular zone (FAZ) size and contour.[3–5] However, quantitative evaluation of the FAZ based on FA is difficult and rarely done in clinical settings, despite the interest and numerous publications on the subject. Optical coherence tomography angiography (OCTA) offers a safer and convenient alternative to FA, and is more amenable to automated quantification, particularly of vascular abnormalities near the fovea, including the FAZ.[6–12]

Numerous methods for quantifying FAZ changes with OCTA in diabetic patients have been investigated, including horizontal and vertical diameter, total two-dimensional area, remodeling, acircularity index (AI), and axis ratio.[13–16] As there is not yet a consensus of how to best quantify the FAZ with OCTA, comparing the clinical utility of FAZ metrics to other measurements of DMI remains difficult. There is also considerable variability of FAZ size and shape in both normal and diabetic patients,[17–22] which may confound the identification of DR-related pathologic changes. In addition, many studies have considered the FAZ in segmented vascular layers, even as the individual plexuses merge at the foveal pit, leading to conclusions about the FAZ size that are more related to segmentation technique than pathologic vascular changes.

One of the major factors affecting FAZ measurements is segmentation of the FAZ boundary. While multiple reports[23–25] have demonstrated high repeatability of semiautomatic FAZ detection using commercial OCTA systems, some studies[26,27] have found significant differences between FAZ detection algorithms and manual delineation. Obtaining accurate FAZ

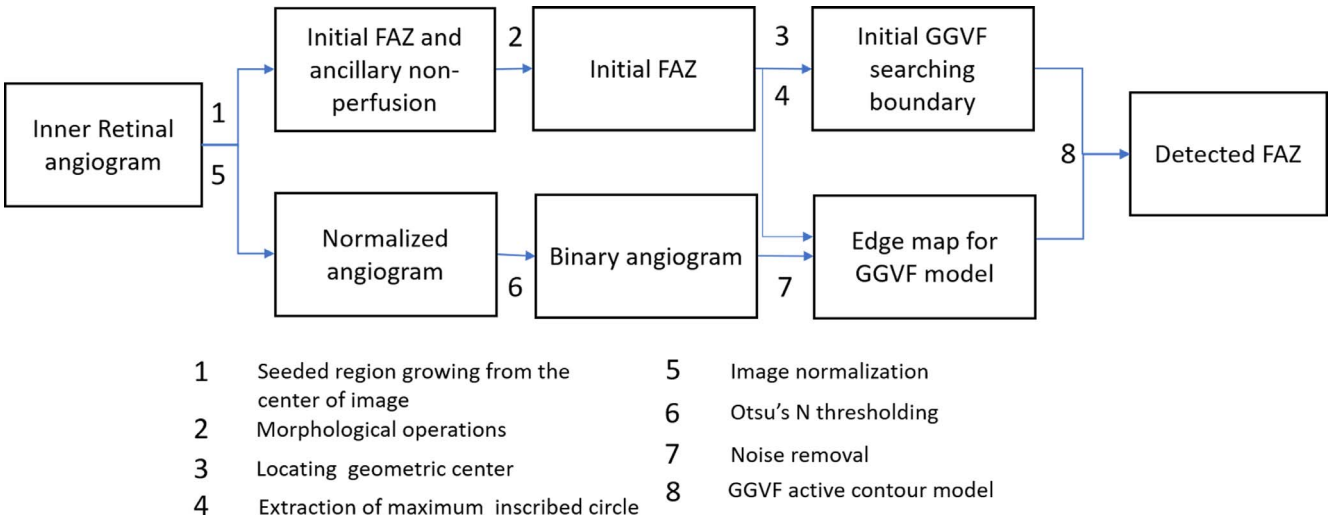

Figure 1. Overview of the proposed algorithm for automatic detection of the FAZ.

segmentation becomes even more difficult in DR, where irregular boundary can result in algorithm failure and inappropriate inclusion or exclusion of abnormal FAZ sections. In this study, we proposed and tested a novel method for automated FAZ identification, based on OCTA using a generalized gradient vector flow (GGVF) snake model. GGVF is an external force for parametric active contours that aids in accurately localizing edges of interest. This model can improve active contour convergence to long, thin boundary indentations by generalizing a diffusion of gradient vectors with two spatially varying weighting functions, while still providing a large capture range.[28–31] Using the GGVF snake model, we evaluated the FAZ based on en face images of the whole inner retina to eliminate the issue of segmentation at the foveal pit. In addition to conventional FAZ metrics including FAZ area and AI, we report two new FAZ metrics that describe the irregularity of FAZ enlargement while partially controlling for physiologic FAZ variation. Finally, we compared the correlation of these FAZ metrics with DR grade and best-corrected visual acuity (BCVA) to that of extrafoveal avascular area (EAA).

Methods

Data Acquisition

Diabetic and healthy control subjects were recruited from the Casey Eye Institute of Oregon Health and Science University (OHSU). This cross-sectional, observational study was approved by the institutional review board of OHSU and complied with the Declaration of Helsinki.[32] Written informed consent was obtained from all study participants. All participants underwent standard ophthalmic examination including assessment of BCVA, using Early Treatment Diabetic Retinopathy Study (ETDRS) charts. ETDRS 7-field color photographs were obtained on all diabetic participants. Eyes with other significant ocular pathology were excluded from the study. The clinician retinopathy severity grading guided the recruitment goals,[33] but masked grading of the color photographs determined eyes to have no retinopathy, mild to moderate nonproliferative diabetic retinopathy (NPDR), or severe NPDR to proliferative diabetic retinopathy for final analysis. Healthy controls had no history or evidence of significant ocular media opacity, age-related macular degeneration, retinal vascular occlusions, or a systemic diagnosis of diabetes mellitus.

OCTA scans were obtained with a commercial spectral-domain OCT system (RTVue-XR; Optovue, Fremont, CA, USA) with an axial scan rate of 70 KHz. This system uses split-spectrum amplitude decorrelation angiography (SSADA) algorithm to detect flow signal efficiently and operates with a scan pattern of two repeated B-scans at 304 raster positions, with each B-scan consisting of 304 A-scans.[14,34] Registration and merging of two consecutive orthogonal scans were applied to form a three-dimensional data cube covering a 3×3 mm^2 area.[35,36] En face OCTA images of the inner retina were generated by maximum projection of the inner retinal slab, which was defined as the slab from the inner limiting membrane to the upper boundary of the outer nuclear layer. Axial length was obtained in all patients with the IOL Master (Carl Zeiss AG, Oberkochen, Germany).

OCTA image exclusion criteria included signal strength index (SSI) below 55, low image quality with eye defocus, and saccade artifacts passing through the FAZ region. Two experienced, independent graders reviewed the OCTA images to assess for the presence of exclusion criteria; disagreements were settled with open discussion between the graders. For patients in whom both eyes met clinical and imaging inclusion criteria, one eye was chosen randomly for study inclusion.

Data Processing

An active contour model that uses GGVF as external forces was applied onto the OCTA images to automatically detect the FAZ (Fig. 1). The GGVF active contour model has advantages in that it has a lower initial contour requirement and is able to more accurately progress into boundary concavities.[31] The algorithm was implemented with custom software written in Matlab 2013a (MathWorks, Natick, MA, USA).

GGVF active contour locates boundaries of shapes in an image by evolving an initial contour driven by external forces defined by a binary edge map along with internal forces. Therefore, the automated algorithm for FAZ quantification consisted of three major components: (1) estimating the initial searching boundary, (2) generating an edge map, and (3) contour evolution with the GGVF snake model. An overview of the algorithm is shown in Figure 1.

The first algorithm component estimates the initial searching boundary by using the following steps: First, the initial FAZ was detected by using a seeded region growing algorithm. A seed was positioned at the image center ($x = 152$, $y = 152$),

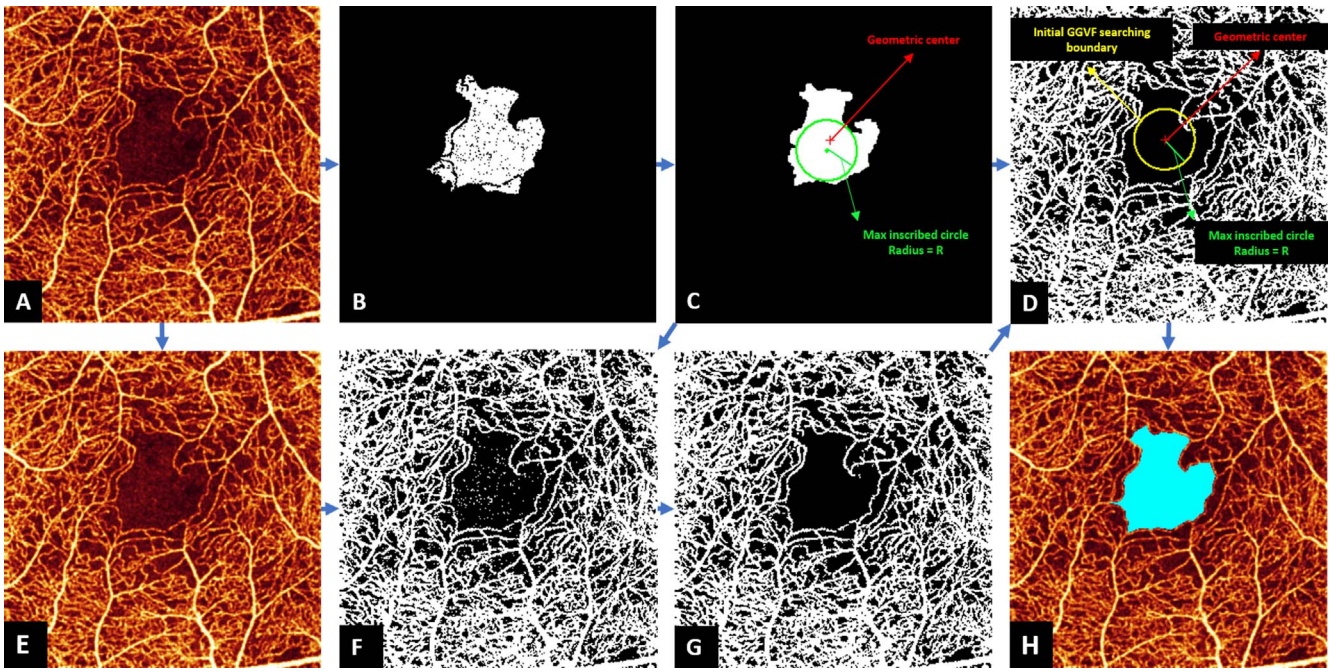

Figure 2. Foveal avascular zone (FAZ) detection in the inner retina of an eye with NPDR eye. The original angiogram (**A**) is processed by seeded region growing from the center of the image to obtain the initial FAZ and ancillary nonperfusion areas (**B**), and morphologic operations removed regions of ancillary nonperfusion (**C**). Locating geometric center was applied to obtain a circle center coordinate (*red dot* in [**C**, **D**]), and extraction of maximum inscribed circle was applied to obtain a radius (*green line* segment in [**C**, **D**]), which was then used to generate the initial GGVF searching boundary (*yellow circle* in [**D**]). The original angiogram (**A**) is normalized to the range [0 1] (**E**) and processed by Otsu's N thresholding (**F**) and noise removal (**G**), which is used to create an edge map for GGVF model (**G**). The initial GGVF searching boundary was then applied on the edge map, and the GGVF active contour model was applied to identify the final FAZ. The resulting final FAZ (*light blue*) is overlaid on the original angiogram (**H**).

growing to a region with similarity larger than 0.02 (Fig. 2B). Next, morphologic operations were used to obtain an initial FAZ (Fig. 2C). The morphologic operations included the following: (1) a $\sqrt{2}$ pixel shrink to remove regions of ancillary nonperfusion that are not continuous with the FAZ; (2) filling the holes in the image; (3) morphologic opening operation with a 4-pixel-wide square kernel to eliminate small regions of signal noise and smooth boundaries; and (4) a 3.5-pixel shrink to obtain an accurate initial curve for the GGVF snake model. These parameters were chosen empirically to obtain a smooth initial FAZ. The n pixel shrink operation aforementioned is based on Euclidean distance transform. For each pixel in the binary image (Fig. 2B), the distance transform assigns a number DT_{xy} that is the distance between that pixel (x, y) and the nearest non-zero pixel (x_1, y_1),[37]

$$DT_{xy} = \min_{x_1 y_1} \sqrt{(x - x_1)^2 + (y - y_1)^2} \qquad (1)$$

and only pixels with $DT_{xy} \leq$ n were kept. Next, the geometric center and radius R of the maximum inscribed circle of the initial FAZ are calculated (Fig. 2C) and used to place a circle centered at the geometric center with radius R (Fig. 2D), which is used as the initial GGVF searching boundary.

To generate the edge map for the GGVF active contour, serial operations were applied, including (1) image normalization: angiogram pixel values were truncated to [0 0.35] and normalized to [0 1] (Fig. 2E); (2) Otsu's N thresholding[38]: eleven ($N = 11$) thresholds were used to divide the angiogram pixels into 12 classes ($C_1, C_2, \ldots, C_{12}$), then classes (C_1, C_2,) were set to 0 and all other classes were set to 1 to generate a binary angiogram (Fig. 2F). Division into a high number of classes results in greater sensitive to low pixel values and is more conducive to retaining complete boundaries than traditional Otsu thresholding; and (3) noise removal: pixels inside the initial FAZ were erased and connected areas smaller than five pixels were eliminated (Fig. 2G).

Finally, with the initial contour and edge map ready, the GGVF active contour model was applied to acquire the contours for the FAZ areas (Fig. 2D).[28–31]

GGVF active contour locates boundaries of shapes in an image by evolving initial contour $X(s) = [x(s), y(s)]$ according to

$$X_t(s,t) = X_{t-1} - \tau\left\{(s,t)\left[\alpha\frac{\partial^2 X_{t-1}}{\partial s^2}(s,t) + \beta\frac{\partial^4 X_{t-1}}{\partial s^2}(s,t)\right] - \mathbf{v}\right\}, \qquad (2)$$

where $x(s)$ and $y(s)$ are x, y coordinates past the contour and s is the normalized index of the control points; τ is the evolution step. $\mathbf{v}$ is GGVF[31]

$$\mathbf{v} = \iint g(|\nabla f|)|\nabla \mathbf{v}|^2 - h(|\nabla f|)(|\mathbf{v} - \nabla f|^2)\,\mathrm{d}x\,\mathrm{d}y, \qquad (3)$$

with $f(x, y)$ being the edge map, $\nabla^2 = \partial^2/\partial \mathrm{x}^2 + \partial^2/\partial \mathrm{y}^2$ being the Laplacian operator, and $g(|\nabla f|) = e^{-\frac{|\nabla f|}{K}}$, $h(|\nabla f|) = 1 - g(|\nabla f|)$.

In the implementation, weighting parameters $\alpha = 0.7, \beta = 0.1$, the iteration number was 60, the evolution step τ was 0.8, and the specification of K determines, to a certain extent, the degree of trade-off between smoothness and gradient consistency. Completion of the GGVF model iterations produces the final detected FAZ (Fig. 2H).

Four FAZ metrics were calculated after automated segmentation of the FAZ (Fig. 3): (1) total FAZ area, (2) AI, defined as

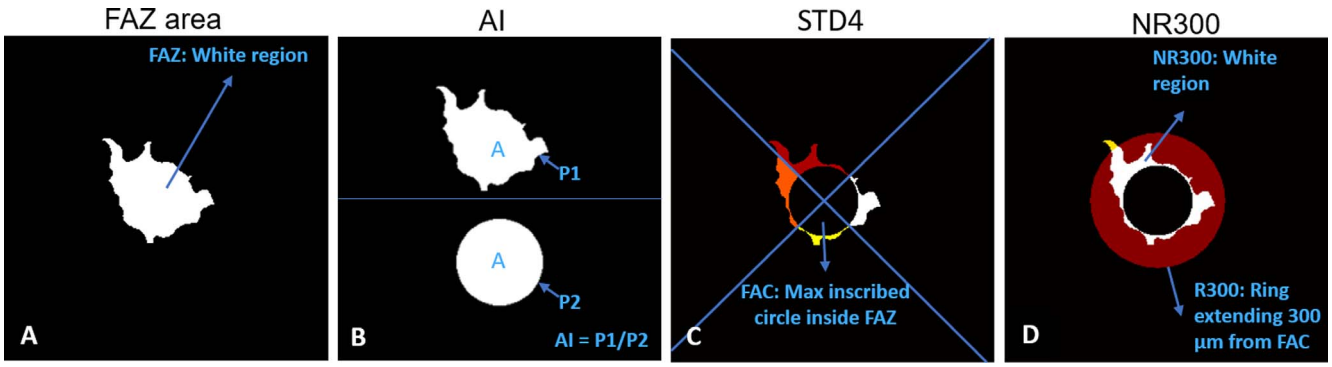

Figure 3. Four quantitative metrics derived from detected FAZ. (**A**) FAZ area. (**B**) Acircularity index (AI), defined as the ratio of perimeter of the FAZ (P1) to the perimeter of a circle equal area (P2).[14] (**C**) STD4, defined as the standard deviation of the area of four sectors of the FAZ after excluding the maximum inscribed circle. (**D**) NR300, defined as the area of intersection of the FAZ with an annular region between the FAZ maximum inscribed circle and outer circle with a radius 300 µm greater than that of the FAZ maximum inscribed circle (R300) divided by the area of the entire annular region.

the ratio of the perimeter of the FAZ to the perimeter of a circle equal area,[14] (3) STD4, defined as the standard deviation of the area of four sectors of the FAZ after excluding the maximum inscribed circle, and (4) NR300, defined as the area of intersection of the FAZ with an annular region between the FAZ maximum inscribed circle and outer circle with a radius 300 µm greater than that of the FAZ maximum inscribed circle (R300) divided by the area of the entire annular region.

$$\mathrm{NR300} = \frac{|\mathrm{FAZ} \cap \mathrm{R300}|}{|\mathrm{R300}|} \quad (4)$$

As previously described, EAA was defined as the total avascular area outside of a 1-mm-diameter circle centered on the fovea.[9] Since we have shown superficial vascular complex (SVC) is primarily damaged by DR,[9,39] in this study, EAA was measured on SVC located at the inner 80% of ganglion cell complex.[9,40] Metrics affected by individual differences in retina magnification including FAZ area, STD4, and EAA were adjusted for the axial length of the eye.

Data Analysis

The FAZ in diabetic and healthy control subjects identified by the automated GGVF snake algorithm was compared with manual grading performed by an experienced grader on the original en face OCT angiograms. The agreement between the automated and manual FAZ areas was assessed by using the Jaccard coefficient, defined as the area of intersection divided by the area of union.

$$J(A,M) = \frac{|A \cap M|}{|A \cup M|}, \quad (5)$$

where A = area of automated segmentation and M = area of manual delineation.

Coefficient of variation was calculated for each FAZ metric in eyes that had two scans with an SSI of 55 or greater to assess within-visit repeatability. To increase the number of eyes available for within-visit repeatability analysis, the second eye of diabetic patients and health controls was included when available.

The Mann-Whitney U test was used to compare FAZ metrics and EAA among patients with various DR severity grades and healthy controls. Spearman correlation coefficients (r_s) were calculated to assess the correlation of each FAZ metric and EAA with DR severity grade and BCVA. The diagnostic accuracy of each parameter was assessed by calculating sensitivity at a fixed specificity of 95%. A P value of less than 0.05 was considered statistically significant. Values were reported as mean (standard deviation). All statistical analysis was performed with SPSS software version 23 (SPSS, Inc., Chicago, IL, USA). P values were adjusted with the Holm-Bonferroni method.

Results

Sixty-six eyes from 66 diabetic patients and 19 control eyes from 19 healthy participants were included (Table 1). As based on clinical exam, eyes from diabetic patients were classified into three groups: no retinopathy ($n = 16$; mean [SD] age, 57 [12] years; 8 women), mild to moderate NPDR ($n = 22$; mean [SD] age, 61 [10] years; 18 women), and severe NPDR or proliferative DR (PDR) ($n = 28$; mean [SD] age, 53 [14] years; 11 women). Eyes from healthy participants were used as controls (n = 19 [22%]; mean [SD] age, 38 [13] years; 13 women). The SSI ranged from 64 to 77 in diabetic eyes without retinopathy, 61 to 81 in mild to moderate NPDR, 60 to 71 in severe NPDR or PDR, and 60 to 87 in controls. Cystoid macular edema was present on macular OCT scans in 8 eyes with mild to moderate NPDR (36.4%) and 11 eyes with severe NPDR or

Table 1. Patient Information

Group	No. of Participants	Age, Mean ± SD	Female, %	VA, ETDRS, Mean ± SD
Healthy controls	19	38 ± 13	68.4	88.42 ± 2.85
Diabetes without DR	16	57 ± 12	50.0	82.69 ± 4.77
Mild to moderate NPDR	22	61 ± 10	81.8	82.00 ± 5.61
Severe NPDR or PDR	28	53 ± 14	39.3	78.25 ± 8.86

VA, visual acuity.

Table 2. Agreement Between Automated Detection and Manual Delineation of Foveal Avascular Zone

Group	Jaccard Similarity Metric	False-Positive Error, mm^2	False-Negative Error, mm^2
Control, $n = 19$	0.87 ± 0.06	0.061 ± 0.035	0.080 ± 0.078
Diabetes without DR, $n = 16$	0.86 ± 0.09	0.079 ± 0.062	0.081 ± 0.123
Mild to moderate NPDR, $n = 22$	0.89 ± 0.05	0.069 ± 0.047	0.042 ± 0.047
Severe NPDR or PDR, $n = 28$	0.83 ± 0.09	0.130 ± 0.097	0.044 ± 0.054

proliferative DR (39.3%). There was very good agreement between automatic and manual detection of the FAZ; the Jaccard coefficient was >0.82 in all subgroups (Table 2). Analysis of within-visit repeatability included the second eye of diabetic patients and healthy controls when available and included 7 diabetic without DR eyes, 13 mild to moderate NPDR eyes, 19 severe NPDR or PDR eyes, and 29 healthy control eyes that had two scans of adequate quality (SSI > 54). There was excellent within-visit repeatability for FAZ area, AI, STD4, and NR300 among all patient subgroups (Fig. 4; Table 3).

Mean FAZ area determined by the automated algorithm in the severe NPDR or PDR group (0.37 ± 0.18 mm^2) was significantly greater than the mean FAZ area in the DM without DR (0.22 ± 0.08 mm^2) and healthy control (0.24 ± 0.12 mm^2) groups, but not the mild to moderate NPDR group (0.30 ± 0.09 mm^2) (Figs. 5, 6). The mean FAZ area in the mild to moderate NPDR group was significantly greater than in the DM without DR group, but not the healthy control group. AI in severe NPDR or PDR eyes (1.39 ± 0.10 mm^2) was significantly greater than AI in the DM without DR (1.29 ± 0.12 mm^2) and healthy control (1.28 ± 0.08 mm^2) groups, but not in the mild to moderate NPDR group (1.33 ± 0.08 mm^2) (Fig. 6). STD4 in severe NPDR or PDR eyes (0.024 ± 0.016 mm^2) was significantly greater than STD4 in the DM without DR (0.012 ± 0.009 mm^2) and healthy control (0.008 ± 0.009 mm^2) groups, but not in the mild to moderate NPDR group (0.017 ± 0.009 mm^2) (Fig. 6). NR300 was significantly different between each subgroup, except when comparing the DM without DR and healthy control groups (Fig. 6). EAA increased significantly with each subgroup (healthy controls: 0.037 ± 0.052 mm^2, DM without DR: 0.107 ± 0.110 mm^2, mild to moderate NPDR: 0.226 ± 0.135 mm^2, severe NPDR or PDR: 0.566 ± 0.385 mm^2) (Figs. 5, 6).

The correlation coefficients between OCTA metrics, DR grade, and BCVA are shown in Table 4. Of the FAZ metrics, NR300 had the strongest correlation ($r_s = 0.703$, $P < 0.001$) with DR grade. None of the FAZ metrics, however, correlated with DR grade as well as EAA ($r_s = 0.807$, $P < 0.001$). Overall, correlations between OCTA metrics and BCVA were weaker, with the strongest two being NR300 ($r_s = -0.424$, $P < 0.001$) and EAA ($r_s = -0.460$, $P < 0.001$). The sensitivity of detecting eyes as abnormal in each DR severity subgroup, compared to healthy controls, while holding specificity at 95% is shown in Table 5 for each OCTA metric. Sensitivity for EAA in differentiating diabetic patients without DR (73%), mild/moderate NPDR (86%), and PDR/severe NPDR (100%) from healthy controls was greater than each FAZ-related OCTA metric.

Discussion

In this study, we described a fully automated method for FAZ identification and quantification using OCTA. This process involves three main parts: (1) preprocessing to minimize residual motion artifacts and background noise and create a binary angiogram; (2) acquiring initial GGVF searching boundary; and (3) applying the GGVF active contour model. This FAZ detection algorithm showed very good agreement with expert manual delineation in healthy control and DR subjects. Data obtained through the automated FAZ detection were used to generate four different FAZ quantitative metrics (FAZ area, AI, STD4, and NR300). All of these metrics showed excellent within-visit repeatability in normal eyes and at all levels of DR severity, and therefore have the potential to serve as reliable tools for the diagnosis of DR and the evaluation of disease progression.

The GGVF snake algorithm was designed to automatically and reliably perform segmentation of the FAZ. In this study, the edge map was a binary image generated from the original angiogram; and the initial GGVF searching boundaries were obtained by using a seeded region growing method, which facilitated a precise capture range and convergence of the GGVF snake to the complex boundary shapes of the FAZ. This fully automated method allows for rapid FAZ delineation and performs well on the more complicated FAZ borders present in advanced DR, where traditional semiautomated algorithms are more likely to fail.

The assessment of DMI and FAZ changes has long been a clinically important process in the risk stratification and management of DR, but rigorous quantification of FA images is rarely performed outside of clinical investigations. Numerous methods for quantifying pathologic changes of the FAZ on OCTA have been proposed[13–16]; some involve measuring the ischemic area, such as FAZ diameter and total area, and others quantify the irregularity of the FAZ shape, such as axis ratio and AI. FAZ enlargement in DR is an asymmetric process,[14,21,41] and therefore assessing both size and shape is likely important for the detection of pathologic change. This may explain why NR300, which incorporates both FAZ area and irregularity, had

Table 3. Within-Visit Repeatability (Coefficient of Variation) of Foveal Avascular Zone Metrics

Quantitative Metrics	Controls, $n = 29$	Diabetes Without DR, $n = 7$	Mild to Moderate NPDR, $n = 13$	Severe NPDR or PDR, $n = 19$
Conventional				
FAZ	0.002	0.000	0.001	0.003
AI	0.013	0.006	0.007	0.008
New				
STD4	0.003	0.001	0.002	0.007
NR300	0.011	0.007	0.004	0.009

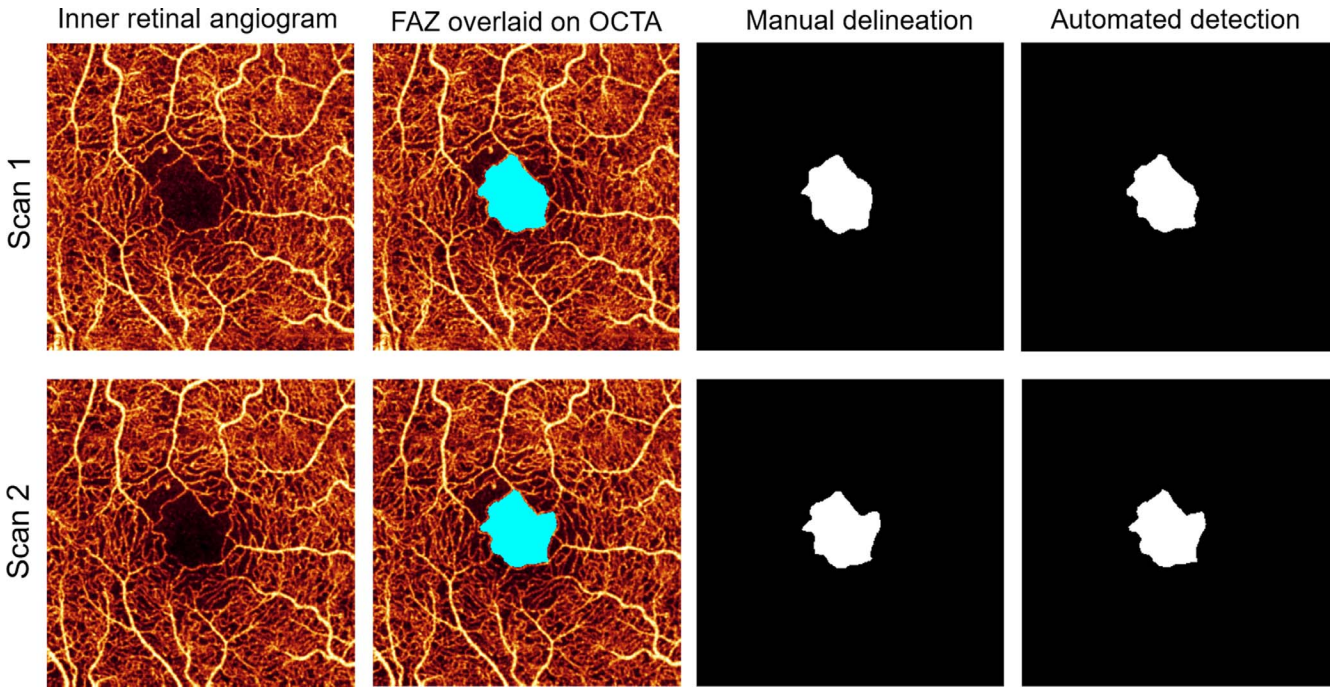

FIGURE 4. Foveal avascular zone determined by the automated algorithm and manual delineation in two intravisit scans from a patient with NPDR.

a stronger correlation with DR severity than FAZ area and AI. Both STD4 and NR300 minimize the effect of normal variation in FAZ size, which likely also contributed to their improved performance. This is accomplished by using a maximum inscribed circle, which partially controls for the original, physiologic FAZ size in each eye. Imaging the FAZ within the inner retinal slab of the OCTA provides the most anatomically meaningful data, as the retinal capillary plexuses merge at the

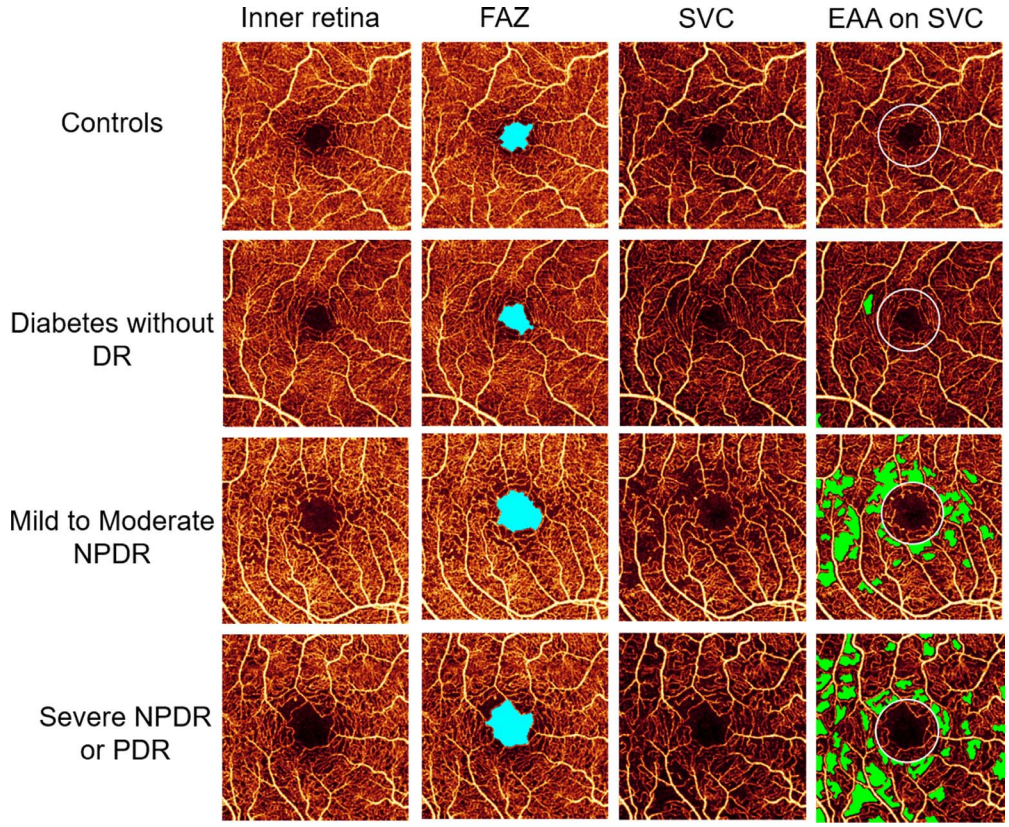

FIGURE 5. Foveal avascular zone (FAZ, *light blue*) detected on inner retinal angiogram and EAA (*green*) detected on SVC in all diabetic retinopathy severity groups.

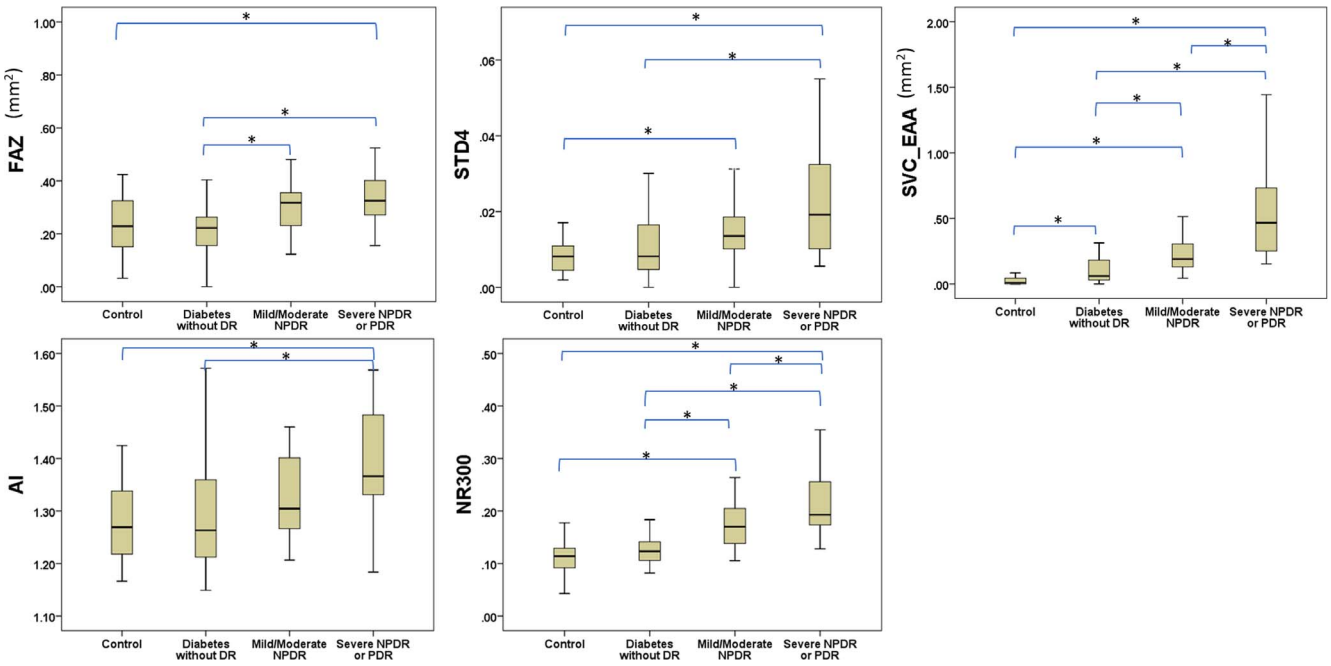

Figure 6. Boxplots showing variation in quantitative foveal avascular zone metrics and extrafoveal avascular area between healthy eyes and varying diabetic retinopathy level. *P* values were adjusted by Holm-Bonferroni method and the significant difference between groups is represented by an asterisk (*).

foveal pit. Additionally, this minimizes segmentation artifact caused by cystoid macular edema, as all retinal capillaries are above the lower segmentation line. While the effect of differences in retinal magnification due to variation in axial length is small and less significant when it changes in an individual patient over time, it should be considered when comparing patient cohorts and defining normative data. Therefore, OCTA metrics affected by absolute scan dimensions were adjusted for individual axial length in this study.

Previously, our group has reported on the detection and quantification of total avascular area, inclusive of the FAZ, using a 6 × 6-mm macular OCTA.[8] Total avascular area analysis reliably detects DR with a high sensitivity and specificity, and is found to be a more reliable biomarker for DR than FAZ area in a small cohort.[8] In another study,[9] differentiation between NPDR and control eyes with avascular area measured with OCTA is greater when a central 1-mm circle is excluded to factor out the normal variation in FAZ area. Additionally, the avascular area in DR patients is greater in the superficial vascular plexus compared with the combined inner retina slab.[9] While FAZ area, AI, STD4, and NR300 were all significantly correlated with DR severity, EAA had a greater sensitivity for detecting DR at all severity levels. Furthermore, in this study we found no significant difference in any of the FAZ metrics between healthy controls and diabetic eyes without DR. Some groups[13,42,43] have reported small but significant changes in FAZ area between these groups, but others[14,44] have reported no significant difference. Some of these divergent results and conclusions may be due to patient selection, study size, and measurement of the FAZ within segmented vascular layers, which can produce results of unclear significance as the individual plexuses merge at the foveal pit. In this study, EAA was the only metric that demonstrated a significant difference between diabetic patients with no clinical evidence of DR and healthy controls.

The findings in this study suggest that other vascular parameters such as EAA may be a better diagnostic tool for DR than FAZ metrics. The most important reason for this is the significant variability in FAZ size in both normal individuals[17–20] and diabetic patients,[21,22] leading to considerable overlap between healthy and disease groups. By comparison, the proportional difference in EAA between healthy and DR subjects is greater, as there is essentially no avascular area outside of the FAZ in healthy eyes. While the maximal inscribed circle methods such as STD4 and NR300 can partially

Table 4. Spearman Correlation Coefficient of Foveal Avascular Zone Metrics and Extrafoveal Avascular Area With Diabetic Retinopathy Grade and Visual Acuity

	Inner				
	Conventional		New		SVC
	FAZ	AI	STD4	NR300	EAA
Correlation with DR severity	0.392**	0.413**	0.487**	0.703**	0.807**
Correlation with VA (ETDRS)	−0.211	−0.285**	−0.274*	−0.424**	−0.460**

* *P* value < 0.05.
** *P* value < 0.01.

Table 5. Sensitivity of Foveal Avascular Zone Metrics and Extrafoveal Avascular Area for the Differentiation of Eyes of Diabetic Patients From Healthy Controls

	Inner				
	Conventional		New		SVC
	FAZ	AI	STD4	NR300	EAA
Diabetes without DR	12%	30%	50%	58%	73%
Mild to moderate NPDR	16%	34%	58%	72%	86%
Severe NPDR or PDR	21%	39%	64%	82%	100%

Sensitivity to detect DR grades with specificity held at 95%.

compensate for the normal FAZ variability, EAA appears to remain a more sensitive biomarker for DR.

The finding that EAA has greater correlation with DR severity, determined by fundus photographic grading with the ETDRS protocol, should not subtract from the clinical significance of FAZ metrics. Current DR grading, using the International Diabetic Retinopathy Severity scale,[33] is based only on clinical fundus appearance and does not directly account for changes to retinal perfusion visible only on FA or OCTA. Regions of DR-related capillary dropout have been associated with local underlying photoreceptor loss,[45–47] and therefore FAZ metrics may be the most relevant to foveal ischemia and central visual potential. While we propose that EAA is a better metric for detecting DR and correlating with the clinical DR severity scale, FAZ measurements may provide useful information on foveal perfusion and visual function. Of the FAZ metrics, NR300 had the strongest correlation with BCVA in this study. We did not control for other factors that could affect visual acuity, including cataract and corneal pathology. Adaptive optics scanning laser ophthalmoscopy, another noninvasive imaging modality that has been used to model hemodynamics within retinal vasculature and assess photoreceptor structural changes in patients with diabetic retinopathy, will likely continue to provide data complementary to that of OCT-based imaging systems.[46,48] Further investigation into the relationship between FAZ metrics, visual acuity, and structural changes in the macula are warranted.

Currently, a tradeoff exists between OCTA image resolution and field of view owing to the limitations in the OCT scan speed. A scan size of 3 × 3-mm was used in this study to maximize FAZ resolution. This scan size allowed for the most accurate FAZ segmentation, but limited the field of view available for EAA detection. A larger field of view with similar resolution may further improve diagnostic accuracy and can be obtained with higher scanning speeds or angiography montaging techniques.

Limitations of this study included the modest number of participants, cross-sectional design, and the use of non–age- or non–sex-matched controls. An association between OCTA vascular density and age has been reported[24]; however, a different study[45] has found no significant relationship between age, sex, and FAZ measurements. Of note, our diabetic cohort may be skewed toward better visual acuity because a higher proportion of patients with poor BCVA were excluded owing to severe imaging artifacts or media opacities. We acknowledge that this principle may limit our ability to determine the true relationship between FAZ metrics, EAA, and visual acuity, particularly at the more severe end of the DR spectrum. While a small study[49] has found no short-term changes in FAZ area after therapy with vascular endothelial growth factor (VEGF) antagonists in eyes with DR, the long-term effects of anti-VEGF agents on FAZ remodeling are unknown and were not investigated in this study. Future comparisons of patients treated with anti-VEGF pharmacotherapy and treatment-naive patients are warranted. Additionally, a small proportion of test cases (5%) had FAZ concavities that were too deep or narrow to be detected by the algorithm. This is due to the algorithm's reliance on an edge map, and FAZ detection may be limited in these rare cases.

Acknowledgments

Supported by Grants R01EY027833, DP3 DK104397, R01 EY024544, P30 EY010572 from the National Institutes of Health (Bethesda, MD, USA), and by unrestricted departmental funding from Research to Prevent Blindness (New York, NY, USA). This work was partially funded by the National Natural Science Foundation of China (No. 61471226), Natural Science Foundation for Distinguished Young Scholars of Shandong Province (No. JQ201516), and the Taishan scholar project of Shandong Province (No. tsqn20161023). Oregon Health & Science University (OHSU), DH, and YJ have a significant financial interest in Optovue, Inc., a company that may have a commercial interest in the results of this research and technology. These potential conflicts of interest have been reviewed and managed by OHSU.

Disclosure: **Y. Lu**, None; **J.M. Simonett**, None; **J. Wang**, None; **M. Zhang**, Optovue, Inc. (E); **T. Hwang**, None; **A.M. Hagag**, None; **D. Huang**, Optovue, Inc. (F, I, R), P; **D. Li**, None; **Y. Jia**, Optovue, Inc. (F), P

References

1. Bresnick GH, De Venecia G, Myers FL, Harris JA, Davis MD. Retinal ischemia in diabetic retinopathy. *Arch Ophthalmol*. 1975;93:1300–1310.
2. Sim DA, Keane PA, Zarranz-Ventura J, et al. The effects of macular ischemia on visual acuity in diabetic retinopathy. *Invest Ophthalmol Vis Sci*. 2013;54:2353–2360.
3. Early Treatment Diabetic Retinopathy Study Research Group. Classification of diabetic retinopathy from fluorescein angiograms: ETDRS report number 11. *Ophthalmology*. 1991;98(suppl 5):807–822.
4. Early Treatment Diabetic Retinopathy Study Research Group. Fluorescein angiographic risk factors for progression of diabetic retinopathy: ETDRS report number 13. *Ophthalmology*. 1991;98(suppl 5):834–840.
5. Mansour AM, Schachat A, Bodiford G, Haymond R. Foveal avascular zone in diabetes mellitus. *Retina*. 1993;13:125–128.
6. Jia Y, Bailey ST, Hwang TS, McClintic SM, Gao SS. Quantitative optical coherence tomography angiography of vascular abnormalities in the living human eye. 2015;112:E2395–E2402.
7. Hwang TS, Jia Y, Gao SS, et al. Optical coherence tomography angiography features of diabetic retinopathy. *Retina*. 2015;35:2371–2376.

8. Hwang TS, Gao SS, Liu L, et al. Automated quantification of capillary nonperfusion using optical coherence tomography angiography in diabetic retinopathy. *JAMA Ophthalmol*. 2016;134:367–373.
9. Zhang M, Hwang TS, Dongye C, Wilson DJ, Huang D, Jia Y. Automated quantification of nonperfusion in three retinal plexuses using projection-resolved optical coherence tomography angiography in diabetic retinopathy. *Invest Ophthalmol Vis Sci*. 2016;57:5101–5106.
10. Kim DY, Fingler J, Zawadzki RJ, et al. Noninvasive imaging of the foveal avascular zone with high-speed, phase-variance optical coherence tomography. *Invest Ophthalmol Vis Sci*. 2012;53:85–92.
11. Ishibazawa A, Nagaoka T, Takahashi A, et al. Optical coherence tomography angiography in diabetic retinopathy: a prospective pilot study. *Am J Ophthalmol*. 2015;160:35–44.e1.
12. Spaide RF. Volume-rendered optical coherence tomography of diabetic retinopathy pilot study. *Am J Ophthalmol*. 2015; 160:1200–1210.
13. De Carlo TE, Chin AT, Bonini Filho MA, et al. Detection of microvascular changes in eyes of patients with diabetes but not clinical diabetic retinopathy using optical coherence tomography angiography. *Retina*. 2015;35:2364–2370.
14. Krawitz BD, Mo S, Geyman LS, et al. Acircularity index and axis ratio of the foveal avascular zone in diabetic eyes and healthy controls measured by optical coherence tomography angiography. *Vision Res*. 2017;139:177–186.
15. Tang FY, Ng DS, Lam A, et al. Determinants of quantitative optical coherence tomography angiography metrics in patients with diabetes. *Sci Rep*. 2017;7:2575.
16. Freiberg FJ, Pfau M, Wons J, Wirth MA, Becker MD, Michels S. Optical coherence tomography angiography of the foveal avascular zone in diabetic retinopathy. *Graefes Arch Clin Exp Ophthalmol*. 2016;254:1051–1058.
17. Bird AC, Weale RA. On the retinal vasculature of the human fovea. *Exp Eye Res*. 1974;19:409–417.
18. Sander B, Larsen M, Engler C, Lund-Andersen H. Absence of foveal avascular zone demonstrated by laser scanning fluorescein angiography. *Acta Ophthalmol (Copenh)*. 1994; 72:550–552.
19. Shahlaee A, Pefkianaki M, Hsu J, Ho AC. Measurement of foveal avascular zone dimensions and its reliability in healthy eyes using optical coherence tomography angiography. *Am J Ophthalmol*. 2016;161:50–55.e1.
20. Chui TY, VanNasdale DA, Elsner AE, Burns SA. The association between the foveal avascular zone and retinal thickness. *Invest Ophthalmol Vis Sci*. 2014;55:6870–6877.
21. Bresnick GH, Condit R, Syrjala S, Palta M, Groo A, Korth K. Abnormalities of the foveal avascular zone in diabetic retinopathy. *Arch Ophthalmol*. 1984;102:1286–1293.
22. Arend O, Wolf S, Jung F, et al. Retinal microcirculation in patients with diabetes mellitus: dynamic and morphological analysis of perifoveal capillary network. *Br J Ophthalmol*. 1991;75:514–518.
23. Lupidi M, Coscas F, Cagini C, et al. Automated quantitative analysis of retinal microvasculature in normal eyes on optical coherence tomography angiography. *Am J Ophthalmol*. 2016;169:9–23.
24. Coscas F, Sellam A, Glacet-Bernard A, et al. Normative data for vascular density in superficial and deep capillary plexuses of healthy adults assessed by optical coherence tomography angiography. *Invest Ophthalmol Vis Sci*. 2016;57:OCT211–OCT223.
25. Carpineto P, Mastropasqua R, Marchini G, Toto L, Di Nicola M, Di Antonio L. Reproducibility and repeatability of foveal avascular zone measurements in healthy subjects by optical coherence tomography angiography. *Br J Ophthalmol*. 2016; 100:671–676.
26. La Spina C, Carnevali A, Marchese A, Querques G, Bandello F. Reproducibility and reliability of optical coherence tomography angiography for foveal avascular zone evalution and measurement in different settings. *Retina*. 2017;37:1636–1641.
27. Linderman R, Salmon AE, Strampe M, Russillo M, Khan J, Carroll J. Assessing the accuracy of foveal avascular zone measurements using optical coherence tomography angiography: segmentation and scaling. *Trans Vis Sci Tech*. 2017; 6(3):16.
28. Kass M, Wikin A, Terzopoulos D. Snakes: active contour models. *Int J Comput Vis*. 1987;1:321–331.
29. Xu C, Prince JL. Gradient vector flow: a new external force for snakes. In: *Proceedings of IEEE Conference on Computer Vision and Pattern Recognition*. New York, NY: IEEE; 1997: 66–71.
30. Xu C, Prince JL. Snakes, shapes, and gradient vector flow. *IEEE Trans Image Process*. 1998;7:359–369.
31. Xu C, Prince JL. Generalized gradient vector flow external forces for active contours. *Signal Process*. 1998;71:131–139.
32. World Medical Association. Declaration of Helsinki: ethical principles for medical research involving human subjects. *J Am Coll Dent*. 2014;81:14–18.
33. Wilkinson CP, Ferris FL III, Klein RE, et al. Proposed international clinical diabetic retinopathy and diabetic macular edema disease severity scales. *Ophthalmology*. 2003;110:1677–1682.
34. Jia Y, Bailey ST, Wilson DJ, et al. Quantitative optical coherence tomography angiography of choroidal neovascularization in age-related macular degeneration. *Ophthalmology*. 2014;121:1435–1444.
35. Kraus MF, Potsaid B, Mayer MA, et al. Motion correction in optical coherence tomography volumes on a per A-scan basis using orthogonal scan patterns. *Biomed Opt Express*. 2012;3: 1182–1199.
36. Kraus MF, Liu JJ, Schottenhamml J, et al. Quantitative 3D-OCT motion correction with tilt and illumination correction, robust similarity measure and regularization. *Biomed Opt Express*. 2014;5:2591–2613.
37. Maurer CR, Rensheng Q, Raghavan V. A linear time algorithm for computing exact Euclidean distance transforms of binary images in arbitrary dimensions. *IEEE Trans Pattern Anal Mach Intell*. 2003;25:265–270.
38. Deepa S, Bharathi S. Efficient ROI segmentation of digital mammogram images using Otsu's N thresholding method. *Int J Eng Res Technol*. 2013;1:51–56.
39. Hwang TS, Zhang M, Bhavsar K, et al. Visualization of 3 distinct retinal plexuses by projection-resolved optical coherence tomography angiography in diabetic retinopathy. *JAMA Ophthalmol*. 2016;134:1411–1419.
40. Campbell JP, Zhang M, Hwang TS, et al. Detailed vascular anatomy of the human retina by projection-resolved optical coherence tomography angiography. *Sci Rep*. 2017;7: 42201.
41. Alipour SH, Rabbani H, Akhlaghi M, Dehnavi AM, Javanmard SH. Analysis of foveal avascular zone for grading of diabetic retinopathy severity based on curvelet transform. *Graefes Arch Clin Exp Ophthalmol*. 2012;250:1607–1614.
42. Dimitrova G, Chihara E, Takahashi H, Amano H, Okazaki K. Quantitative retinal optical coherence tomography angiography in patients with diabetes without diabetic retinopathy. *Invest Ophthalmol Vis Sci*. 2017;58:190–196.
43. Di G, Weihong Y, Xiao Z, et al. A morphological study of the foveal avascular zone in patients with diabetes mellitus using

optical coherence tomography angiography. *Graefes Arch Clin Exp Ophthalmol*. 2016;254:873–879.

44. Simonett JM, Scarinci F, Picconi F, et al. Early microvascular retinal changes in optical coherence tomography angiography in patients with type 1 diabetes mellitus. *Acta Ophthalmol*. 2017;95:e751–e755.
45. Scarinci F, Jampol LM, Linsenmeier RA, Fawzi AA. Association of diabetic macular nonperfusion with outer retinal disruption on optical coherence tomography. *JAMA Ophthalmol*. 2015;133:1036–1044.
46. Nesper PL, Scarinci F, Fawzi AA. Adaptive optics reveals photoreceptor abnormalities in diabetic macular ischemia. *PLoS One*. 2017;12:e0169926.
47. Sawides L, Sapoznik KA, de Castro A, et al. Alterations to the foveal cone mosaic of diabetic patients. *Invest Ophthalmol Vis Sci*. 2017;58:3395–3403.
48. Lu Y, Bernabeu MO, Lammer J, et al. Computational fluid dynamics assisted characterization of parafoveal hemodynamics in normal and diabetic eyes using adaptive optics scanning laser ophthalmoscopy. *Biomed Opt Express*. 2016; 7:4958–4973.
49. Ghasemi Falavarjani K, Iafe NA, Hubschman JP, Tsui I, Sadda SR, Sarraf D. Optical coherence tomography angiography analysis of the foveal avascular zone and macular vessel density after anti-VEGF therapy in eyes with diabetic macular edema and retinal vein occlusion. *Invest Ophthalmol Vis Sci*. 2017;58:30–34.

Investigative Ophthalmology & Visual Science